

determining the balance between Si and N uptake by the biological community. □

Received 29 July 1997; accepted 21 February 1998.

- Martin, J. H. & Fitzwater, S. E. Iron deficiency limits phytoplankton growth in the north-east Pacific subarctic. *Nature* **331**, 341–343 (1988).
- Coale, K. H. *et al.* A massive phytoplankton bloom induced by an ecosystem-scale iron fertilization experiment in the equatorial Pacific Ocean. *Nature* **383**, 495–501 (1996).
- de Baar, H. J. W. *et al.* On iron limitation of the Southern Ocean: experimental observations in the Weddell and Scotia Seas. *Mar. Ecol. Prog. Ser.* **65**, 105–122 (1990).
- Hutchins, D. A. in *Progress in Phycological Research* Vol. II (eds Chapman, D. & Round, F.) 1–49 (Biopress, Bristol, 1995).
- Bruland, K. W., Donat, J. R. & Hutchins, D. A. Interactive influences of bioactive trace metals on biological production in oceanic waters. *Limnol. Oceanogr.* **36**, 1555–1577 (1991).
- Chavez, F. P. *et al.* Phytoplankton variability in the central and eastern tropical Pacific. *Deep-Sea Res.* **43**, 835–870 (1996).
- DiTullio, G. R., Hutchins, D. A. & Bruland, K. W. Interaction of iron and major nutrients controls phytoplankton growth and species composition in the tropical north Pacific Ocean. *Limnol. Oceanogr.* **38**, 495–506 (1993).
- Sharp, J. H. Improved analysis for 'particulate' organic carbon and nitrogen from seawater. *Limnol. Oceanogr.* **19**, 984–989 (1974).
- Brzezinski, M. A. The Si:C:N ratio of marine diatoms: interspecific variability and the effect of some environmental variables. *J. Phycol.* **21**, 347–357 (1985).
- Geider, R. J. & LaRoche, J. The role of iron in phytoplankton photosynthesis, and the potential for iron-limitation of primary productivity in the sea. *Photosyn. Res.* **39**, 275–301 (1994).
- Martin, J. H. in *Primary Productivity and Biogeochemical Cycles in the Sea* (eds Falkowski, P. G. & Woodhead, A. D.) 123–137 (Plenum, New York, 1992).
- Handbook of Chemistry and Physics* 63rd edn (eds Weast, R. C. & Astle, M. J.) (CRC, Boca Raton, 1982).
- Dugdale, R. C., Wilkerson, F. P. & Minas, H. J. The role of a silicate pump in driving new production. *Deep-Sea Res.* **42**, 697–719 (1995).
- Dugdale, R. C. & Wilkerson, F. P. Silicate regulation of new production in the eastern equatorial Pacific. *Nature* **391**, 270–273 (1998).
- Martin, J. H., Gordon, R. M., Fitzwater, S. & Broenkow, W. W. VERTEX: phytoplankton/iron studies in the Gulf of Alaska. *Deep-Sea Res.* **36**, 649–680 (1989).
- Minas, H. J. & Minas, M. Net community production in 'High Nutrient-Low Chlorophyll' waters of the tropical and Antarctic Oceans: grazing versus iron hypothesis. *Ocean. Acta* **15**, 145–162 (1992).
- de Baar, H. J. W. *et al.* Importance of iron for plankton blooms and carbon dioxide drawdown in the Southern Ocean. *Nature* **373**, 412–415 (1995).
- Harrison, P. J., Conway, H. L., Holmes, R. W. & Davis, C. O. Marine diatoms grown in chemostats under silicate or ammonium limitation. III. Cellular composition and morphology of *Chaetoceros debilis*, *Skeletonema costatum* and *Thalassiosira gravida*. *Mar. Biol.* **43**, 19–31 (1977).
- Hutchins, D. A., DiTullio, G. R. & Bruland, K. W. Iron and regenerated production: evidence for biological iron recycling in two marine environments. *Limnol. Oceanogr.* **38**, 1242–1255 (1993).
- Muggli, D. L., Lecourt, M. & Harrison, P. J. Effects of iron and nitrogen source on the sinking rate, physiology and metal composition of an oceanic diatom from the subarctic Pacific. *Mar. Ecol. Prog. Ser.* **132**, 215–227 (1996).
- Mortlock, R. A. *et al.* Evidence for lower productivity in the Antarctic Ocean during the last glaciation. *Nature* **351**, 220–223 (1991).
- Charles, C. D., Froelich, P. N., Zibello, M. A., Mortlock, R. A. & Morley, J. J. Biogenic opal in Southern Ocean sediments over the last 450,000 years: implications for surface water chemistry and circulation. *Paleoceanography* **6**, 697–728 (1991).
- Rue, E. L. & Bruland, K. W. The role of organic complexation on ambient iron chemistry in the equatorial Pacific Ocean and the response of a mesoscale iron addition experiment. *Limnol. Oceanogr.* **42**, 901–910 (1997).
- Bruland, K. W., Franks, R. P., Knauer, G. A. & Martin, J. H. Sampling and analytical methods for the determination of copper, cadmium, zinc and nickel at the nanogram per liter level in sea water. *Anal. Chim. Acta* **105**, 233–245 (1979).

Acknowledgements. We thank M. Sanderson, C. De La Rocha, Y. Zhang, M. Schwartz, G. Smith, M. Brzezinski, V. Franck, N. Fisher, P. Harrison, D. Kirchman, S. Wilhelm, A. Witter and the captain and crew of the RV *Pt. Sur*. This work was supported by NSF Chemical and Biological Oceanography and University of Delaware Research Foundation funding.

Correspondence and requests for material should be addressed to D.A.H. (e-mail address: dahutch@udel.edu).

Anisotropic structures at the base of the Earth's mantle

Lev Vinnik*†, Ludovic Breger*‡ & Barbara Romanowicz*‡

* *Seismological Laboratory and ‡ Department of Geology and Geophysics, University of California, Berkeley, California 94720, USA*

† *Institute of Physics of the Earth, Bolshaya Gruzinskaya 10, Moscow CIS*

The D'' shell at the base of the Earth's mantle is thought to be a thermal and compositional boundary layer where vigorous dynamical processes are taking place^{1–4}. An important property of D'' is its seismic anisotropy, expressed as different velocities for horizontally and vertically polarized shear waves that have been diffracted or reflected at the core–mantle boundary^{5,6}. The nature of this anisotropy has been the subject of debate^{7–11}.

Here we present an analysis of various seismic phases, generated in the Kermadec–Fiji–Tonga zone and recorded at stations in North America, which reveal a region at the base of the mantle beneath the southwest Pacific Ocean where horizontally propagating vertically polarized waves are slower (by at least 10 per cent) than horizontally polarized waves. This observed anisotropy is an order of magnitude larger than that previously thought to exist in the lower mantle, and corresponds to lateral variations in horizontally polarized shear-wave velocity which are also of about 10 per cent. We speculate that this anisotropy may be the result of the mixing and shearing of strongly heterogeneous material in the boundary layer.

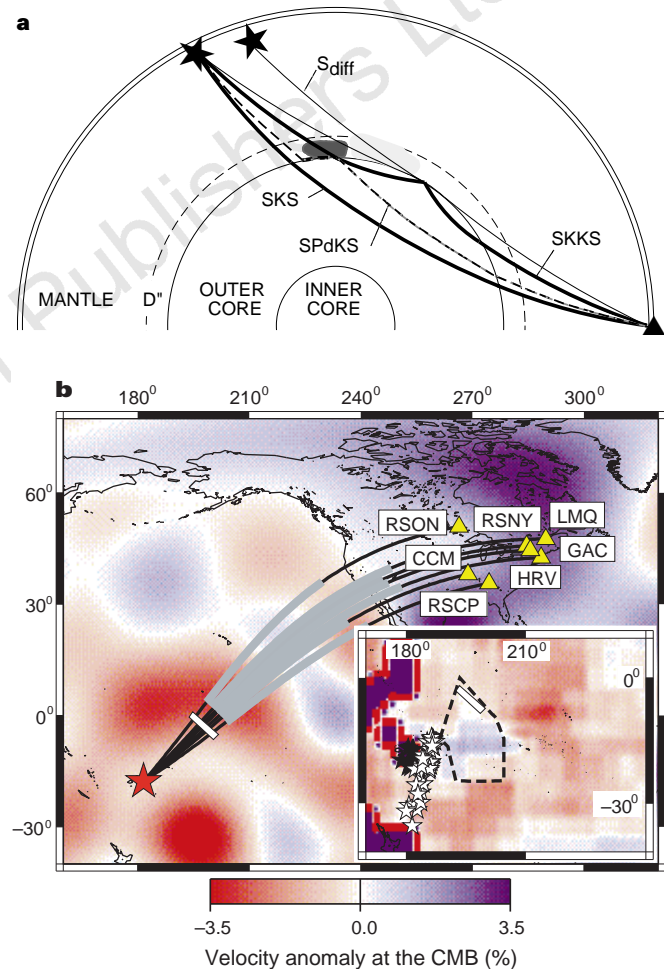


Figure 1 Geometry of the data set considered. **a**, Schematic representation of the wave paths of SKS, SKKS, S_{diff} and SPdKS. The wave paths of S_{diff} for two different positions of the source (stars) differ only at the source side. The lightly shaded area indicates the region where SH is slow, as discussed in the text. The darker, hatched area is the region where SH velocity is elevated or normal, but SV is much slower than SH. **b**, Surface projections of wave paths superimposed on a tomographic model of SH velocity in D'' (ref. 15). The light-grey zone of the wave path indicates approximately the D'' leg of S_{diff} for the shortest distances considered. The white bar corresponds to the kink for S_{diff}-SKS residuals, discussed in the text. Red star is location of earthquake source region; yellow triangles and 3/4-letter codes indicate station locations and names, respectively. Inset, close-up look at the source side of the wave-paths. Epicentres of deep Fiji–Tonga events and of shallow Kermadec–Fiji–Tonga events are shown by filled and open stars, respectively. The background tomographic model of S-wave velocity in D'' is from ref. 16. The polygon indicates the zone of ultra-low P-wave velocity in D'' (ref. 18). The barcode indicates amplitudes of shear velocity anomalies at the core–mantle boundary (CMB) in the tomographic models^{15,18}.

The first part of our analysis is based on the residuals of differential travel times between seismic phases SH_{diff} and SKS/SKKS relative to those for the standard Earth model PREM¹². (SH_{diff} are horizontally polarized S waves that have been diffracted at the core–mantle boundary; SKS/SKKS are shown in Fig. 1.) Differential travel times are helpful because they are not sensitive to errors in focal parameters of seismic events and structural complexities in the source region. Contrary to earlier studies^{13,14}, we consider (1) not the absolute values of the residuals, but rather the slopes of the resulting time–epicentral distance plots; (2) not the average residuals for many stations, but the individual slope for every station; and (3) not only the residuals for deep events, but also for intermediate and shallow events. For the given source–receiver geometry (Fig. 1) and a fixed station, changes of the wave path occur practically only at the source side of the wave path.

The residuals as a function of epicentral distance show a remarkable trend, consistent from station to station, for shallow and deep events and whether SKS or SKKS is used as reference phase. Figure 2 shows examples for the three best stations. Each panel can be divided into two parts, with rapidly increasing residuals at shorter distances, and slowly rising (or decreasing) residuals at larger distances. To make this trend more visible, we divide each set of measurements into two subsets corresponding to epicentral distances smaller than or equal to, and greater than or equal to, a variable cut-off distance. When the best-fitting position of the cut-off and linear fits on both sides of it are obtained by regression, the average variance reduction is twofold with respect to a single regression line. We note that the epicentral distance of the change of slope (the ‘kink’) varies (for example, 116–117° at HRV; 103–104° at RSON), depending on the epicentral distance range of the Kermadec–Fiji–Tonga seismic zone to the given station. Comparable results are obtained for the other stations where a similar analysis was performed: RSCP, LMQ, RSNY and GAC (Fig. 1).

The features in Fig. 2 cannot be explained by mantle complexity immediately beneath the seismic foci, because the change of slope is

present in the data for both deep and shallow events. Therefore, our preferred explanation for the kink is a first-order change in the properties of the lowermost mantle at the source side of the wave-path. Moreover, SKS and SKKS ray-paths are separated in D'' by a distance exceeding 10°, and a similar trend in the residuals in Fig. 2 with respect to SKS and SKKS implies that the effect is mainly in the travel times of SH_{diff} . If the position of the kink for every station is inverted for the position of the corresponding border in the D'' layer, assuming that SH enters D'' at a height of 300 km above the core–mantle boundary, the estimates for different stations are mutually consistent and correspond to the white bar in Fig. 1b. In experiments with synthetic seismograms, the anomaly of slowness of 1.1 s per degree corresponds to S-wave velocity in D'' reduced by ~10% with respect to PREM. The region of anomalously low SH-wave velocity is located to the northeast of the bar (Fig. 1b), whereas SH velocity to the southwest of the bar is either slightly elevated or normal. Qualitatively, this division is confirmed by two recent tomographic models^{15,16} (Fig. 1b), but the magnitude of the low-velocity anomaly in both models is ~3 times smaller than in our data. Robustness of our technique is confirmed by other data¹⁷.

The residuals of SKKS–SKS differential travel times relative to PREM, derived from our data (Fig. 3) are positive, with an average value of around 2–3 s. As argued in ref. 18, these positive residuals can only be explained by anomalously low S-wave velocity in the lowermost mantle on the source side, due to the longer paths of SKKS relative to SKS. Our data, however, indicate that, on the source side, SKS and SKKS propagate in a region of D'' with normal SH velocity (Fig. 1b). As SKS and SKKS are SV polarized, to explain the discrepancy at least partly, we suggest that although SH velocity is normal, SV velocity in the lowermost mantle on the source side is anomalously low. (SV indicates vertically polarized S waves.)

To obtain quantitative estimates of this anisotropy, we assume that the lowermost mantle is intrinsically isotropic, finely layered and horizontally stratified. For long waves, it behaves like a homogeneous transversely isotropic medium with a vertical axis of

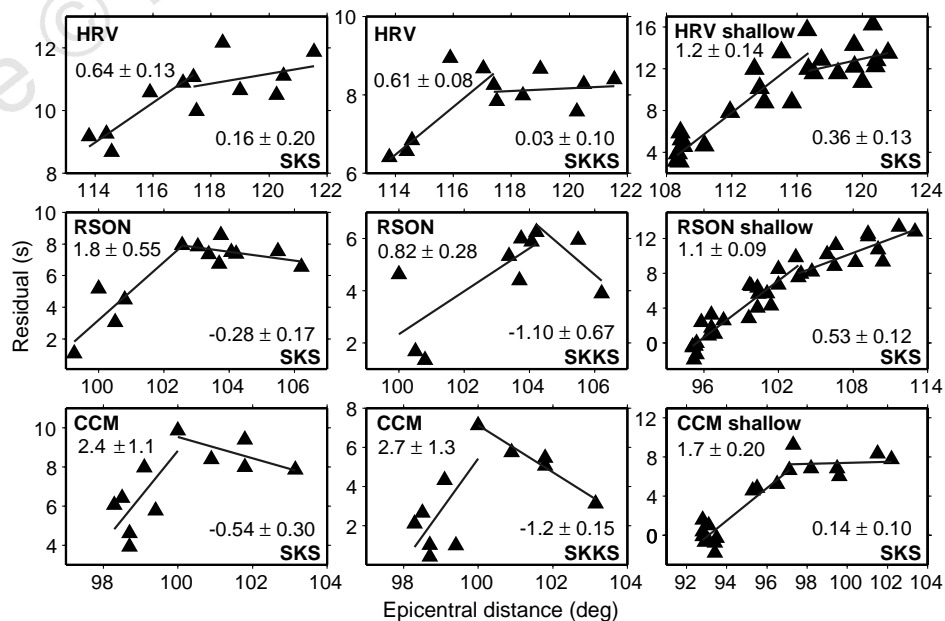


Figure 2 Residuals of SH_{diff} –SKS and SH_{diff} –SKKS differential travel times with respect to those for PREM¹², for HRV/WFM, RSON and CCM, and corresponding regression lines. The data labelled ‘shallow’ are for shallow and intermediate events; all others are for deep events. Shallow events broaden the distance interval available for SKS. The slopes of the plots are controlled mainly by the slowness of SH_{diff} and, consequently, by SH velocity at the source side of D'' . The slope is negative, positive or equal to zero, if SH velocity is higher, lower or similar

to that in PREM. Numerical values of the slopes of the regression lines with their respective confidence intervals are shown in the upper left and lower right corners of each panel. Confidence intervals are usually around ± 0.1 – 0.3 s per degree, but they exceed ± 1.0 s per degree for deep events at CCM, left of the kink. If the latter data are excluded, the average values of the slopes are 1.12 ± 0.2 and -0.21 ± 0.2 s per degree, left and right of the kink, respectively.

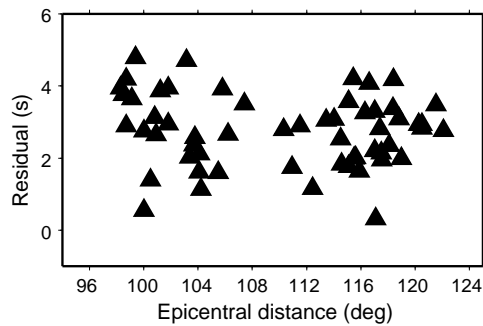


Figure 3 SKKS-SKS residuals for all paths in Fig. 1b. Comparable residuals were reported for similar wave-paths in earlier studies^{13,18,24}. For other paths beneath the Pacific and America, the residuals are close to zero^{18,24}.

symmetry^{19–21}. In this medium, SH_{diff} and SV_{diff} propagate independently, with the former faster than the latter, which is consistent with the seismic observations⁵. To explain residuals of ~ 2 s, SKS and SKKS velocities in a layer 300 km thick should be $\sim 10\%$ lower than standard velocity. For the angles of incidence characteristic of SKS and SKKS, the SV velocities are larger than for horizontal propagation. Then the difference between SH and SV velocities for horizontal propagation can be even higher than 10%. This prediction can be tested by observing propagation of SH_{diff} and SV_{diff} .

The seismic phase SV_{diff} is usually weak, and can be easily distorted by effects of azimuthal anisotropy in the mantle outside D'' and side refraction of SH_{diff} . To eliminate these effects and to pick arrivals of SV_{diff} accurately, we have devised a special technique²², illustrated in ref. 22 for the records of HRV/WFM and RSON. For the present study, a search for SV_{diff} has been conducted in the records of the deep Fiji-Tonga events at seismograph stations shown in Fig. 1b. The best data set has been obtained at HRV/WFM, RSON and CCM. Remarkable features of the detected SV_{diff} signals are their distance-dependent delays relative to SH_{diff} (Fig. 4). At shorter distances, the slopes of the plots are close to 0 s per degree, whereas at larger distances they are in the range 1.0–1.6 s per degree. Then anisotropy is weak (not more than a few per cent) in the region of very low SH velocity (northeast of the white bar in Fig. 1b), and $\sim 15\%$ in the region of normal SH velocity, southwest of the bar. Anisotropy of $\sim 15\%$ is stronger by about an order of magnitude than reported elsewhere.

Additional data on the properties of D'' beneath the southwest Pacific are provided by the observations of SPdKS (Fig. 1a). This phase propagates as P_{diff} in D'' and as SKS elsewhere²³. P_{diff} beneath the southwest Pacific is anomalously slow^{18,24}, with a remarkable correlation between the anomalous delays of SPdKS relative to SKS and positive SKKS-SKS residuals, similar to those shown in Fig. 3. An explanation for this phenomenon is partial melting²⁵. The anomalously slow P_{diff} , however, propagates on the source side in a medium with normal SH velocity (Fig. 1b), which is hard to reconcile with a strong reduction of S velocity, expected in the case of partial melting. Because, as we have demonstrated, the SKKS-SKS residuals can be related to anisotropy, the correlation between them and SPdKS delays suggests that the delays are affected by anisotropy as well. Moreover, east of the white bar in Fig. 1b, where (according to our data) anisotropy is weak, the layer of low P-wave velocity, if present, is very thin²⁶. Assuming that the SPdKS delays are related to anisotropy, we note that the low horizontal P-wave velocity in a fine-layered horizontally stratified medium is possible if the variations of S-wave velocity between the layers are much stronger than those of P-wave velocity²⁰. Another possibility to be considered is lattice preferred orientation²⁷.

For normal distribution of random variations of S-wave velocity in the stack of thin horizontal layers with mean m and standard

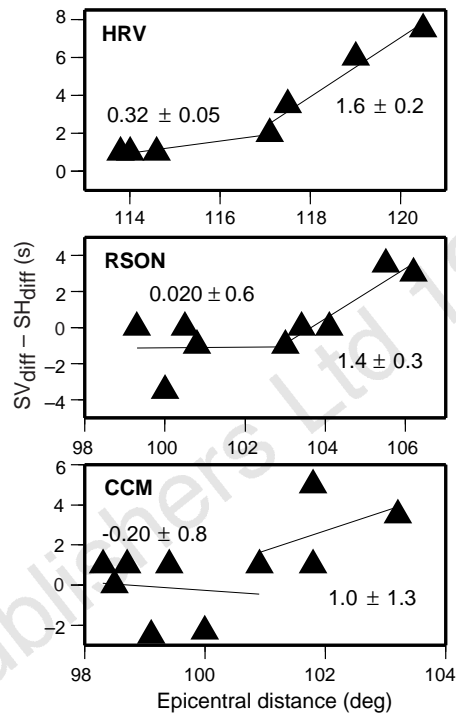


Figure 4 Delays of SV_{diff} with respect to SH_{diff} as a function of epicentral distance for stations HRV/WFM, RSON and CCM. The slope of any of the plots is the difference in slowness between SV_{diff} and SH_{diff} at the source side of the wave-path. Magnitude of anisotropy can be determined as the ratio between these slopes, and the standard slowness of 8.4 s per degree. Each data set is approximated by two regression lines. The boundaries between the corresponding distance intervals are taken from Fig. 2. Numerical values of the slopes of the regression lines with their respective confidence intervals are shown adjacent to the corresponding portions of the plots.

deviation σ , the SH/SV velocity ratio for horizontal propagation is expressed²⁰ as $SH/SV \approx \sqrt{1 + 4(\sigma/m)^2}$. For S-wave anisotropy of 15%, σ thus evaluated is 28% of m . It is not possible to explain the variations exceeding a few per cent solely by temperature variations²⁸. S-wave velocity can be significantly lowered by partial melting or/and by accumulation of crystalline iron-alloy products of chemical reactions between iron of the outer core and mantle perovskite²⁹. Among these possibilities, relatively weak variations of P-wave velocity favour partial melting. The layered structure in D'' could be generated by convective mixing and shearing. Then, strong anisotropy in D'' should be accompanied by strong wave scattering. The anomalous region of D'' , if projected on the surface of the Earth, is close to Polynesia, a region of unusual thermal agitation, where a large-scale thermochemical plume may be present at the top of the lower mantle³⁰. The anisotropic region in D'' could somehow be related to the same plume.

Comparable magnitudes of lateral heterogeneity and anisotropy suggest that lateral variations of anisotropy can be mistaken for lateral velocity variations, when the models are derived under the assumption of isotropy. Whatever its origin, the observations of strong and laterally variable anisotropy add a new dimension to the question of properties and processes in the D'' layer. \square

Received 27 March 1997; accepted 19 March 1998.

1. Doornbos, D. J., Spiliopoulos, S. & Stacey, F. D. Seismological properties of D'' and the structure of a thermal boundary layer. *Phys. Earth Planet. Inter.* **41**, 225–239 (1986).
2. Knittle, E. & Jeanloz, R. Earth's core-mantle boundary: results of experiment at high pressures and temperatures. *Science* **251**, 1438–1443 (1991).
3. Kellogg, L. H. & King, S. D. Effect of mantle plumes on the growth of D'' by reaction between the core and mantle. *Geophys. Res. Lett.* **20**, 379–382 (1993).

4. Loper, D. E. & Lay, T. The core-mantle boundary region. *J. Geophys. Res.* **100**, 6397–6420 (1995).
5. Vinnik, L., Farra, V. & Romanowicz, B. Observational evidence for diffracted SV in the shadow of the Earth's core. *Geophys. Res. Lett.* **16**, 519–522 (1989).
6. Lay, T. & Young, C. J. Analysis of seismic SV waves in the core's penumbra. *Geophys. Res. Lett.* **18**, 1373–1376 (1991).
7. Maupin, V. On the possibility of anisotropy in the D'' layer as inferred from the polarization of diffracted S-waves. *Phys. Earth Planet. Inter.* **87**, 1–32 (1994).
8. Vinnik, L., Romanowicz, B., Le Stunff, Y. & Makeyeva, L. Seismic anisotropy in the D'' layer. *Geophys. Res. Lett.* **22**, 1657–1660 (1995).
9. Kendall, J. M. & Silver, P. G. Constraints from seismic anisotropy on the nature of the lowermost mantle. *Nature* **381**, 409–412 (1996).
10. Matzel, E., Sen, S. E. & Grand, S. P. Evidence for anisotropy in the deep mantle beneath Alaska. *Geophys. Res. Lett.* **23**, 2416–2420 (1996).
11. Garnero, E. & Lay, T. Lateral variations in lowermost mantle shear wave anisotropy beneath the north Pacific and Alaska. *J. Geophys. Res.* **102**, 8121–8135 (1996).
12. Dziewonski, A. M. & Anderson, D. L. Preliminary Reference Earth Model. *Phys. Earth Planet. Inter.* **25**, 297–356 (1981).
13. Schweitzer, J. & Mueller, G. Anomalous difference traveltimes and amplitude ratios of SKS and SKKS from Fiji-Tonga events. *Geophys. Res. Lett.* **13**, 1529–1532 (1986).
14. Garnero, E. & Helmberger, D. V. Travel times of S and SKS: implication for three-dimensional lower mantle structure beneath the central Pacific. *J. Geophys. Res.* **98**, 8225–8241 (1993).
15. Li, X. D. & Romanowicz, B. Global mantle shear velocity model developed using nonlinear asymptotic coupling theory. *J. Geophys. Res.* **101**, 22245–22272 (1996).
16. Grand, S., van der Hilst, R. & Widiyantoro, S. Global seismic tomography: a snapshot of convection in the Earth. *GSA Today* **7**, 1–7 (1997).
17. Breger, L., Romanowicz, B. & Vinnik, L. Test of tomographic model of D'' using differential travel time data. *Geophys. Res. Lett.* **25**, 5–8 (1998).
18. Garnero, E. & Helmberger, D. V. Seismic detection of a thin laterally varying boundary layer at the base of the mantle beneath the central-Pacific. *Geophys. Res. Lett.* **23**, 977–980 (1996).
19. Backus, G. E. Long-wave elastic anisotropy produced by horizontal layering. *J. Geophys. Res.* **67**, 4427–4440 (1962).
20. Nevsky, M. V. *Quasianisotropy of Velocities of Seismic Waves* (Nauka, Moscow, 1974). (in Russian).
21. Levin, F. K. Seismic velocities in transversely isotropic media. *Geophysics* **44**, 918–936 (1979).
22. Vinnik, L., Breger, L. & Romanowicz, B. On the inversion of Sd particle motion for anisotropy in D''. *Geophys. Res. Lett.* **25**, 679–682 (1998).
23. Kind, R. & Mueller, G. Computations of SV waves in realistic Earth models. *J. Geophys.* **41**, 142–162 (1975).
24. Garnero, E. & Helmberger, D. V. A very slow basal layer underlying large-scale low-velocity anomalies in the lower mantle beneath the Pacific; evidence from core phases. *Phys. Earth Planet. Inter.* **91**, 161–176 (1995).
25. Williams, Q. & Garnero, E. Seismic evidence for partial melt at the base of Earth's mantle. *Science* **273**, 1528–1530 (1996).
26. Mori, J. & Helmberger, D. V. Localized boundary layer below the mid-Pacific velocity anomaly identified from a PcP precursor. *J. Geophys. Res.* **100**, 20359–20365 (1995).
27. Karato, S. I. Seismic anisotropy in the deep mantle, boundary layers and the geometry of mantle convection. *Pure Appl. Geophys.* **151**, 565–587 (1998).
28. Wyssession, M. E., Okal, E. A. & Bina, C. R. The structure of the core-mantle boundary from diffracted waves. *J. Geophys. Res.* **97**, 8749–8764 (1992).
29. Jeanloz, R. in *Relating Geophysical Structures and Processes, The Jeffreys Volume* 121–127 (*Geophys. Monogr.* **76**, Am. Geophys. Union, Washington DC, 1993).
30. Vinnik, L., Chevrot, S. & Montagner, J. P. Evidence for a stagnant plume in the transition zone? *Geophys. Res. Lett.* **24**, 1007–1011 (1997).

Acknowledgements. We thank M. Wyssession for reviews. This work was partially supported by NSF.

Correspondence and requests for materials should be addressed to B.R. (e-mail: barbara@seismo.berkeley.edu).

Ediacara-type fossils in Cambrian sediments

Sören Jensen, James G. Gehling* & Mary L. Droser†

Department of Earth Sciences, University of Cambridge, Downing Street, Cambridge CB2 3EQ, UK

* University of South Australia, Warrendi Road, The Levels, South Australia 5095, Australia

† Department of Earth Sciences, University of California, Riverside, California 92521-0423, USA

Fossil assemblages that preserve soft-bodied organisms are essential for our understanding of the composition and diversity of past life. The worldwide terminal Proterozoic Ediacara-type fossils (from ~600–544 Myr BP) are unique in consisting of soft-bodied animals, which are typically preserved as impressions in coarse-grained sediments^{1–4}. These Lagerstätten are also special because they pre-date the major burst of skeletonization, which occurred near the start of the Cambrian period³. Most Ediacara-type fossils are interpreted to be cnidarians, but higher metazoans such as annelids and molluscs may also be represented^{1–4}. However, the unique style of preservation and difficulties in finding convincing

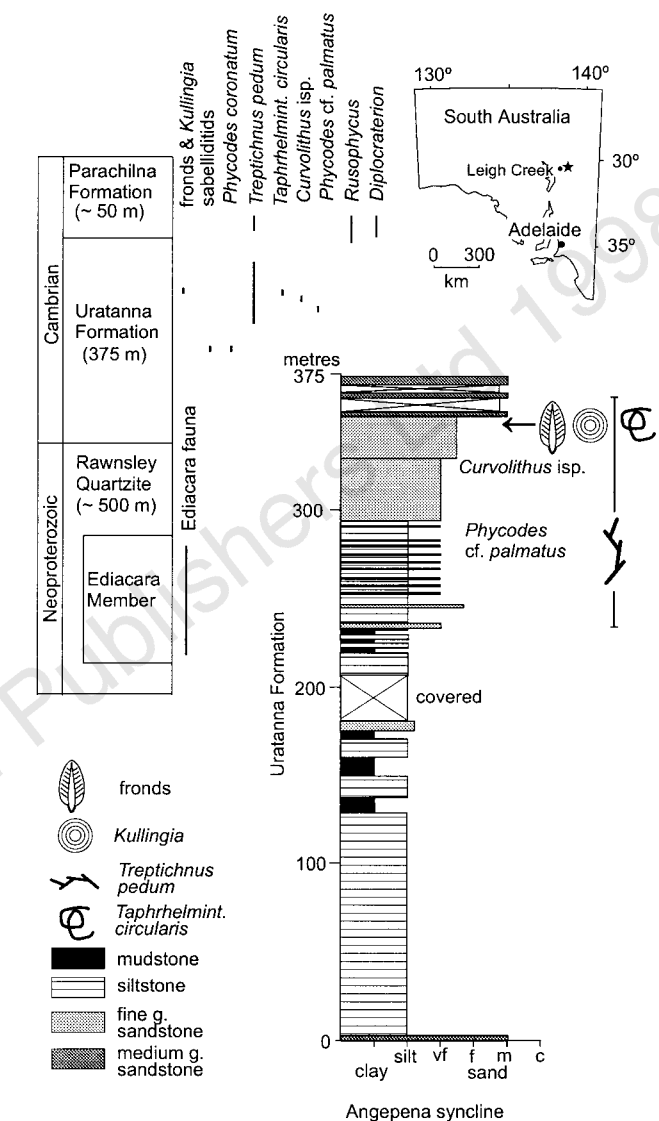


Figure 1 Location (marked by an asterisk, top right) and stratigraphic context of Ediacara-type fronds from the Uratanna Formation, in the Angepena syncline, northern Flinders Ranges. The simplified lithological log (bottom left and right) shows the occurrence of fronds and *Kullingia* and the distribution of selected trace fossils. The stratigraphical context of the Uratanna Formation and a range of selected faunal elements is shown schematically (top left). g, grained; vf, very fine; f, fine; m, medium; c, coarse.

morphological homologies with definite animals have led some specialists to prefer non-metazoan interpretations, such as Vendobionta⁵. In addition, the rarity of Ediacara-type fossils in younger sediments has led to suggestions of a terminal Proterozoic mass extinction⁶. Here we report typical Ediacara-type frond-shaped fossils that occur together with an assemblage of Cambrian-type trace fossils in unequivocally Cambrian-aged sediments of the Uratanna Formation, South Australia. This occurrence bridges the apparent divide between the terminal Proterozoic and Cambrian fossil assemblages, and also suggests that closure of a taphonomic window (an interval of time with unique preservational conditions) was as important as extinction in the disappearance of Ediacara-type organisms.

One of the great controversies in animal evolution concerns the significance of the worldwide terminal Proterozoic soft-bodied Ediacaran fauna^{1–5}. The traditional interpretation of these fauna as including early representatives of Phanerozoic phyla such as